Report

Current Biology

Laminar Organization of Working Memory Signals in Human Visual Cortex

Highlights

- Early visual cortex contains item-specific working memory signals
- Working-memory-related activity is strongest in the agranular layers of V1
- Working-memory-related activity is present at all depths in V2 and V3

Authors

Samuel J.D. Lawrence, Tim van Mourik, Peter Kok, Peter J. Koopmans, David G. Norris, Floris P. de Lange

Correspondence

floris.delange@donders.ru.nl

In Brief

Using high-field MRI, Lawrence et al. show that holding a visual item in working memory leads to top-down activation of the primary visual cortex. This activity is strongest in the agranular layers. These results provide new insights into how bottom-up and top-down signals are deployed in visual cortex.

Lawrence et al., 2018, Current Biology *28*, 1–6
November 5, 2018
https://doi.org/10.1016/j.cub.2018.08.043

CellPress

Please cite this article in press as: Lawrence et al., Laminar Organization of Working Memory Signals in Human Visual Cortex, Current Biology (2018), https://doi.org/10.1016/j.cub.2018.08.043

Current Biology
Report

Laminar Organization of Working Memory Signals in Human Visual Cortex

Samuel J.D. Lawrence,[1] Tim van Mourik,[1] Peter Kok,[2] Peter J. Koopmans,[3] David G. Norris,[1,3] and Floris P. de Lange[1,4,*]
[1]Donders Institute for Brain, Cognition and Behaviour, Radboud University Nijmegen, 6525 Nijmegen, the Netherlands
[2]Department of Psychology, Yale University, New Haven, CT 06511, USA
[3]Erwin L. Hahn Institute for Magnetic Resonance Imaging, University Duisburg-Essen, Essen, Germany
[4]Lead Contact
*Correspondence: floris.delange@donders.ru.nl
https://doi.org/10.1016/j.cub.2018.08.043

SUMMARY

The human primary visual cortex (V1) is not only activated by incoming visual information but is also engaged by top-down cognitive processes, such as visual working memory, even in the absence of visual input [1–3]. This feedback may be critical to our ability to visualize specific visual features, as higher-order regions lack the selectivity to represent such information [4]. Clearly, such internally generated signals do not trigger genuine perception of the remembered stimulus, meaning they must be organized in a manner that is different to bottom-up-driven signals. Internally generated signals may be kept separate from incoming sensory data by virtue of the laminar organization of inter-area cortical connections. Namely, bottom-up driving connections target layer 4, located in the middle of the cortical column, and feedback connections target deep and superficial layers and avoid layer 4 [5–7]. Using lamina-resolved fMRI, we simultaneously measured the activity in three early visual cortical areas (V1–V3) that are recruited to represent stimulus information during visual working memory [8]. We observed item-specific working memory signals in early visual cortex. In V1, this item-specific activity was selectively present at deep and superficial cortical depths, avoiding the middle layers, and working-memory-related activity was present at all depths in V2 and V3. These results show for the first time the laminar organization of internally generated signals during visual working memory in the human visual system and provide new insights into how bottom-up and top-down signals in visual cortex are deployed.

RESULTS

We measured the laminar organization of internally generated signals in V1 formed during visual working memory. To this end, we employed a laminar fMRI analysis method [9] (van Mourik et al., 2015, ISMRM, abstract; see STAR Methods for further details) to measure depth-specific blood-oxygen-level-dependent (BOLD) responses from primary (V1) and extrastriate (V2 and V3) visual cortex of twenty-one subjects during a visual working memory task in which subjects had to keep in mind a specific orientation (see Figure 1).

To examine stimulus-specific activity across visual cortex during visual working memory, we divided visually responsive cortical regions into sub-populations depending on their orientation preference and measured response differences between sub-populations during working memory [10]. Specifically, we measured the orientation preference of each voxel (0.8 mm isotropic) in visual cortex, using an orientation localizer scan in which subjects viewed clockwise- (45°) and counter-clockwise (135°)-oriented gratings, isolating a total of 1,000 voxels that most strongly preferred the clockwise (500 voxels) or counter-clockwise (500 voxels) stimulus in V1–V3 separately (also see Figure S1). By separately analyzing subsets of voxels that were selective for opposite orientations, we were able to examine activity time courses in voxels preferring the maintained and discarded stimulus during visual working memory.

Laminar Organization of Internally Generated Signals in V1–V3

On each trial of the working memory task (Figure 1), subjects were presented with two sample oriented gratings and cued to hold one of the sample orientations in memory. Following an 11.5-s working memory interval, subjects judged whether a probe stimulus was oriented slightly clockwise or counter-clockwise relative to the cued stimulus orientation. The mean discrimination threshold was 7.0° (SD = 3.3) at an average performance level of 77.6% correct (SD = 6.3%; task difficulty was staircased to target 75% correct performance), indicating subjects were able to maintain the cued orientation in working memory with high precision. Figure 2A shows the average single trial BOLD time course from voxels that preferred the orientation held in memory and voxels that preferred the discarded orientation, averaged across gray matter layers. Voxels that preferred the orientation held in memory exhibited a significantly larger sustained response during the working memory interval (highlighted by the shaded region in Figure 2A) compared to voxels that preferred the orthogonal orientation (V1: $F[1, 20] = 12.47$, $p = 0.002$; V2: $F[1, 19] = 5.23$, $p = 0.034$; V3: $F[1, 19] = 5.49$, $p = 0.030$).

We next examined how this sustained item-selective activity, a known signal of working memory [10, 11], was organized

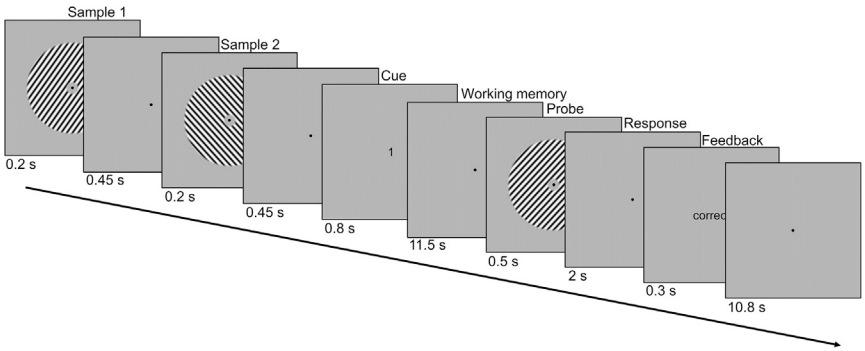

Figure 1. Stimulus Presentation Scheme for the Visual Working Memory Task

On each trial, subjects were presented with two sample orientations—one clockwise and one counter-clockwise—and subsequently provided with a retro-cue that instructed them which of the two orientations to maintain in memory. A probe stimulus followed the 11.5-s working memory interval. Subjects judged whether the probe was oriented clockwise or counter-clockwise with respect to the stimulus they held in working memory. They were provided with feedback at the end of each trial.

across cortical depth. In effect, this described which cortical depths contained item-specific information that described the orientation being maintained in working memory.

Figure 2B shows how the average response difference between voxels that preferred the remembered item and voxels that preferred the discarded item during visual working memory was organized across cortical depth in V1–V3. The laminar organization of this item-specific activity varied across the visual areas we examined ($F [3.23, 61.28] = 3.78$; $p = 0.013$). Specifically, item-specific working memory activity varied across depths in V1 ($F [2, 40] = 4.46$; $p = 0.018$), being larger at superficial ($t [20] = 3.61$; $p = 0.002$) and deep ($t [20] = 2.40$; $p = 0.027$) cortical depths compared to middle depths. Conversely, the same laminar activity profiles were uniform in V2 ($F [2, 38] = 1.93$; $p = 0.160$) and V3 ($F [2, 38] = 1.61$; $p = 0.213$), not showing any differences across depth. Internally generated information about the orientation held in working memory, therefore, was selective to deep and superficial cortical depths in V1, while item-specific working memory activity was equally strong across all depths in V2 and V3.

Laminar Organization of Bottom-Up Signals in V1–V3

As a point of comparison, we quantified the laminar organization of stimulus selectivity evoked by externally generated signals (i.e., visual stimulation). Although feedforward connections largely target layer 4, bottom-up signals quickly propagate to other cortical depths within ~20 ms [12, 13]. Given that fMRI provides an aggregate of activity accrued over multiple seconds, we predicted that stimulus selectivity during visual stimulation should be relatively uniform across depth compared to item-specific visual working memory activity, similar to the depth profiles of bottom-up responses reported in other laminar fMRI studies [9, 14–16]. To address this question, we inspected the laminar profile of activity during our orientation localizer, in which clockwise and counter-clockwise orientations were presented in a block design (Figure S1). The average response during a block of visual stimulation is shown in Figure 3A separately for voxels that preferred the presented orientation (preferred) and voxels that preferred the orthogonal orientation (non-preferred). Note that these are shown only to aid visualization and were not interrogated statistically, as the amplitude of the response difference between preferred and non-preferred is potentially artificially enhanced by our voxel selection procedure derived from the same data. How this response difference was organized across cortical depths, however, is orthogonal to its overall amplitude and as such not affected by any inflation from the voxel selection procedure. We therefore interrogated the laminar organization of bottom-up signals, but not their amplitude, statistically.

We found differences in laminar selectivity profiles between regions ($F [4, 76] = 2.75$; $p = 0.034$): although there were no differences in selectivity across depth in V1 ($F [2, 40] = 0.44$; $p = 0.648$) and V2 ($F [2, 38] = 2.20$; $p = 0.125$), there was a trend of increasing selectivity from deep to superficial depths in V3 ($F [2, 38] = 4.70$; $p = 0.015$), resulting in a significant difference between deep and superficial selectivity ($t [19] = 3.05$; $p = 0.007$) in this area. The monotonic increase in stimulus selectivity from deep to superficial cortical depths in V3 shares a similar laminar profile with a known bias in BOLD signal strength, which gets stronger toward the cortical surface due to venous blood draining [17–20], which we also observed in this study (see Figure S2). Within V1, the laminar profile of stimulus-specific activity during visual stimulation was distinct from the profile of item-specific activity during visual working memory ($F [2, 38] = 4.33$; $p = 0.020$). This indicates that the laminar organization of stimulus information in V1 was dependent on whether it was induced by internally or externally generated signals.

DISCUSSION

We investigated the laminar organization of internally generated neural signals during visual working memory in human early visual cortex. We observed strong item-specific activity in V1–V3, corroborating earlier research [8, 21]. Interestingly, this working memory activity was selectively present at deep and superficial, but not middle, cortical depths within V1, while it was equally strong across all depths in V2 and V3. Additionally, this activity profile was specific to the internal generation of images: we observed no such variation across depth in V1 when visual cortex was stimulated by external stimuli.

These results are consistent with the notion that visual working memory is supported by feedback from higher order brain areas that specifically targets the agranular layers of V1. It is now well established from multivariate decoding studies that patterns of activity in V1 during maintenance of a particular orientation are similar to those elicited by perception of the same orientation [8, 21]. This has been interpreted as evidence that orientation columns in V1 are recruited to represent detailed information about a remembered or imagined stimulus [8, 22], presumably because higher order brain areas involved in memory lack the receptive field properties to represent such local visual information [4]. While we similarly observe a strong neural overlap

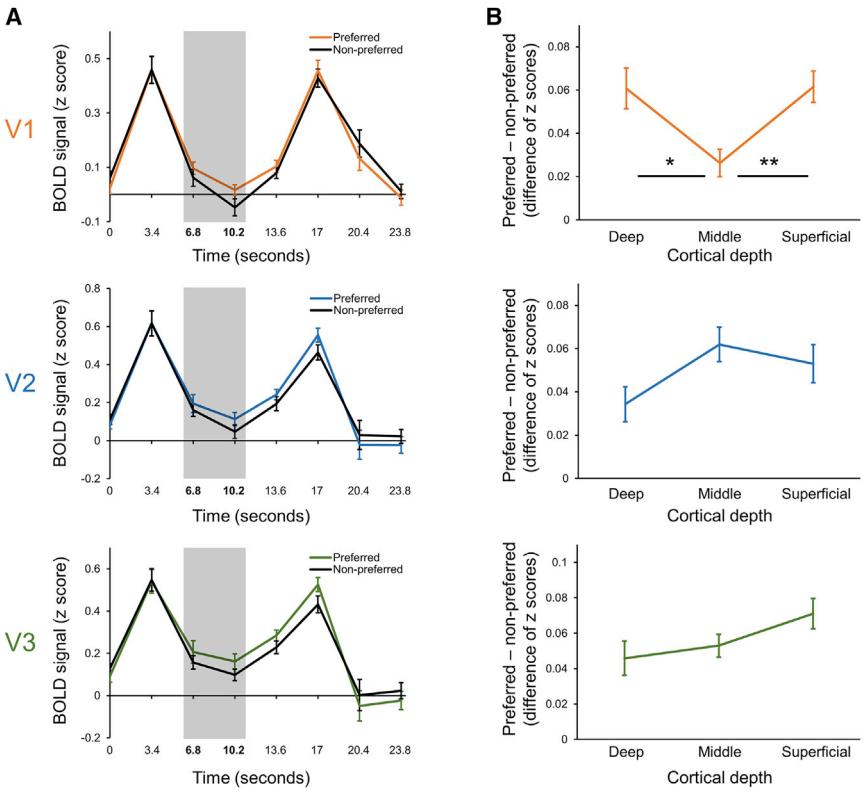

Figure 2. Laminar Organization of Internally Generated Signals in V1–V3

(A) Average BOLD response for a single trial of the visual working memory task in voxels that preferred the orientation held in memory (colored line) and voxels that preferred the orthogonal orientation (black line), averaged across gray matter layers for V1–V3 (top, middle, and bottom, respectively). The working memory delay stretched over the measurements taken at 3.4, 6.8, and 10.2 s; however, we only include the highlighted measurements at 6.8 and 10.2 s in our estimation of working memory activity, as the response at 3.4 s was likely to include activity relating to the sample stimuli presented at the beginning of the trial. Data in (A) are baselined to the average response across preferred and non-preferred voxels at the end of the trial (23.8 s).

(B) Depth-specific breakdown of stimulus selectivity during working memory, calculated by taking the difference between the preferred and non-preferred responses during interval highlighted in (A). Asterisks denote significant paired-samples t tests (*$p < 0.05$; **$p < 0.01$).

In all panels, error bars show within-subject SE. See also Figure S1 for more on the selection and properties of functional masks, Figure S2 for overall BOLD activation across cortical depth, and Figure S3 for individual subject data.

between perception and working memory in visual circuits, our results point to a possibly important marker that can differentiate between these processes: bottom-up stimulation activates the entire cortical column, whereas working memory selectively activates the agranular layers of V1.

Our results provide two important novel findings. First, we show that the maintained representation of specific visual features (i.e., orientation) during working memory selectively engages the agranular layers of V1. Similarly, a recent study showed that the active maintenance of a targets' spatial location is associated with spiking activity and current sinks in agranular layers of monkey V1 [12]. We therefore show the laminar profile of spatial working memory activity [12] can be generalized to both the human visual cortex and to working memory for visual features as opposed to spatial location. Second, we add that the laminar profile of working memory activity is not uniform across visual areas. Namely, we find that, in contrast to V1, working memory signals were equally strong across cortical depths in extrastriate areas V2 and V3. Although this may seem surprising at first, this behavior may naturally follow from the increased spiking activity in superficial layers of V1 during working memory [12]. That is, neurons in the superficial layers of V1 that project to layer 4 of V2 [23, 24] could activate the middle layer of downstream cortical areas. This interpretation suggests that, during our task, orientation columns in V1 were recruited through top-down feedback to store the to-be-maintained stimulus, and this stimulus information was subsequently fed up through the visual hierarchy to inform a decision. Consistent with this notion, modulations from spatial attention in monkey V4 engage the entire cortical column and are in fact largest in input layer 4 [25]. This could be caused by top-down attentional modulations that amplify visually evoked signals earlier in the system, for example, V1 (or even the lateral geniculate nucleus [26]), which in turn amplifies the feedforward signal that targets the input layer 4 of V4. Similarly, feedback modulations related to contour grouping are selectively present in deep and superficial layers of V1 but affect the entire cortical column in V2 [27].

It is possible that feedback specifically targeted V1 in our study because the visual feature subjects had to maintain was orientation—a feature that V1 neurons are exquisitely tuned to [28]. This leaves an intriguing avenue for future research whereby one might devise a visual working memory task designed to target extrastriate cortex. A task involving the retrieval of more complex visual features, such as angles, curves, or whole objects, might result in feedback that targets extrastriate visual areas with receptive fields more suited to representing these more complex features. In line with this notion, Koyano et al. [29] trained monkeys to perform a visual working memory task on object identity and found an accompanying increase in activity selective to deep layers of temporal cortex, which is known to be selective for such objects [30, 31]. This suggests that, when monkeys were required to maintain the identity of an object, temporal neurons with complex receptive fields capable of representing whole objects were recruited through top-down feedback.

The laminar profile of internally generated activity is relevant for neurocomputational models of perceptual inference, such as predictive coding [32–35]. Predictive coding posits that the brain constructs an internal model of the world, encoding the possible causes of sensory inputs as parameters of a generative

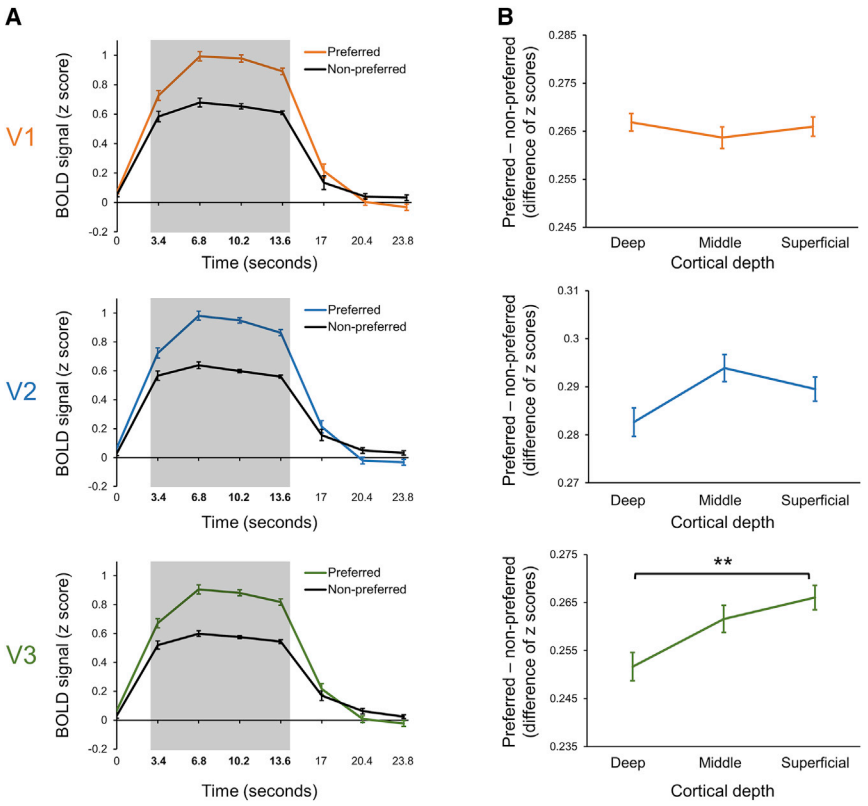

Figure 3. Laminar Organization of Bottom-Up Signals in V1–V3

(A) Average block BOLD response for the orientation localizer in voxels that preferred the presented orientation (colored line) and voxels that preferred the orthogonal orientation (black line), averaged across gray matter layers for V1–V3 (top, middle, and bottom, respectively). Responses during visual presentation are highlighted by the shaded region. Data are baselined to the average response at the end of a trial (23.8 s), averaged across preferred and non-preferred.

(B) Depth-specific breakdown of stimulus selectivity during visual presentation, calculated by taking the difference between the preferred and non-preferred responses during the interval highlighted in (A). Asterisks denote significant paired-samples t tests (**$p < 0.01$).

In all panels, error bars show within-subject SE. See also Figure S1 for more on the selection and properties of functional masks, Figure S2 for overall BOLD activation across cortical depth, and Figure S3 for individual subject data.

model. Feedback connections carry predictions of expected neural activity in the lower cortical area (or "virtual input"), which can be compared to bottom-up input, resulting in optimal perceptual inference. Our findings suggest that the virtual input created by the generative model resides in the deep and superficial layers of the cortical column and avoids the middle layer. These observations appear in line with a recent detailed analysis of the canonical microcircuits for predictive coding [36].

Our results demonstrate the feasibility of measuring depth-dependent BOLD responses using high-resolution fMRI. Nevertheless, it should be noted that several methodological challenges remain [19, 24], such as BOLD activity biases toward the pial veins and the mixing of signals across depth bins due to laminar partial voluming. Although the depth-specific responses we report should be interpreted within the influence of spatial vascular dynamics, we believe that our results are less likely to be tainted by these issues for several reasons. First, our dependent variable was the response difference between two conditions (rather than overall BOLD activity, which was indeed biased toward superficial layers; see Figure S2), which revealed a V-shaped laminar activity profile that is distinct from the pattern exhibited by venous draining artifacts. Second, we employed a spatial generalized linear model (GLM) method that helps to separate responses across cortical bins and estimate depth-specific responses (van Mourik et al., 2015, ISMRM, abstract). This approach has been shown to result in responses that are less correlated across cortical depths compared to interpolation approaches [9] and correct for laminar partial voluming [37]. Third, we show a dissociation between the laminar profiles of top-down, internally generated activity and bottom-up, stimulus-evoked activity, which precludes a simple explanation based on biases in signal or sequence. Finally, the laminar profiles we report for working memory and visual stimulation using BOLD are highly consistent with those reported using electrophysiological techniques [12]. It therefore seems more likely that our results reflect the laminar organization of neural processing during working memory as opposed to spatial hemodynamics.

In conclusion, using high-resolution laminar fMRI, we identified a working memory signal that was selectively present at deep and superficial, but not middle, cortical depths in V1. Our results indicate that internally generated information about specific visual features is formed by feedback to the agranular layers of V1. These findings provide new insights in the laminar circuits involved in internally generated signals in the early visual system.

STAR★METHODS

Detailed methods are provided in the online version of this paper and include the following:

- KEY RESOURCES TABLE
- CONTACT FOR REAGENT AND RESOURCE SHARING
- EXPERIMENTAL MODEL AND SUBJECT DETAILS
- METHOD DETAILS
  - Retinotopic Mapping
  - Psychophysical procedure
  - fMRI data acquisition
  - Preprocessing of fMRI data
  - Coregistration of anatomical and functional data
- QUANTIFICATION AND STATISTICAL ANALYSIS
  - Definition of functional masks
  - Univariate approach to measuring working memory activity

SUPPLEMENTAL INFORMATION

Supplemental Information includes three figures and can be found with this article online at https://doi.org/10.1016/j.cub.2018.08.043.

ACKNOWLEDGMENTS

We are grateful to Alexis Joyaux for assistance with data collection. This work was supported by the Netherlands Organisation for Scientific Research (NWO Vidi grant 452-13-016) and the EC Horizon 2020 Program (ERC starting grant 678286; "Contextvision"), both awarded to F.P.d.L., and the Spinoza Grant SPI 40-118 supporting T.v.M.

AUTHOR CONTRIBUTIONS

All authors designed the study. S.J.D.L. programmed the stimuli. S.J.D.L. and P.J.K. collected the data. S.J.D.L., T.v.M., and F.P.d.L. analyzed the data. T.v.M. wrote the laminar analysis tools. All authors wrote the manuscript.

DECLARATION OF INTERESTS

The authors declare no competing interests.

Received: July 5, 2018
Revised: August 7, 2018
Accepted: August 20, 2018
Published: October 18, 2018

REFERENCES

1. Markov, N.T., Misery, P., Falchier, A., Lamy, C., Vezoli, J., Quilodran, R., Gariel, M.A., Giroud, P., Ercsey-Ravasz, M., Pilaz, L.J., et al. (2011). Weight consistency specifies regularities of macaque cortical networks. Cereb. Cortex *21*, 1254–1272.
2. Muckli, L., and Petro, L.S. (2013). Network interactions: non-geniculate input to V1. Curr. Opin. Neurobiol. *23*, 195–201.
3. Roelfsema, P.R., and de Lange, F.P. (2016). Early visual cortex as a multiscale cognitive blackboard. Annu. Rev. Vis. Sci. *2*, 131–151.
4. Pasternak, T., and Greenlee, M.W. (2005). Working memory in primate sensory systems. Nat. Rev. Neurosci. *6*, 97–107.
5. Felleman, D.J., and Van Essen, D.C. (1991). Distributed hierarchical processing in the primate cerebral cortex. Cereb. Cortex *1*, 1–47.
6. Rockland, K.S., and Virga, A. (1989). Terminal arbors of individual "feedback" axons projecting from area V2 to V1 in the macaque monkey: a study using immunohistochemistry of anterogradely transported Phaseolus vulgaris-leucoagglutinin. J. Comp. Neurol. *285*, 54–72.
7. Anderson, J.C., and Martin, K.A.C. (2009). The synaptic connections between cortical areas V1 and V2 in macaque monkey. J. Neurosci. *29*, 11283–11293.
8. Harrison, S.A., and Tong, F. (2009). Decoding reveals the contents of visual working memory in early visual areas. Nature *458*, 632–635.
9. Kok, P., Bains, L.J., van Mourik, T., Norris, D.G., and de Lange, F.P. (2016). Selective activation of the deep layers of the human primary visual cortex by top-down feedback. Curr. Biol. *26*, 371–376.
10. Albers, A.M., Meindertsma, T., Toni, I., and de Lange, F.P. (2018). Decoupling of BOLD amplitude and pattern classification of orientation-selective activity in human visual cortex. Neuroimage *180*, 31–40.
11. Christophel, T.B., Klink, P.C., Spitzer, B., Roelfsema, P.R., and Haynes, J.D. (2017). The distributed nature of working memory. Trends Cogn. Sci. *21*, 111–124.
12. Van Kerkoerle, T., Self, M.W., and Roelfsema, P.R. (2017). Layer-specificity in the effects of attention and working memory on activity in primary visual cortex. Nat. Commun. *8*, 13804.
13. Self, M.W., van Kerkoerle, T., Supèr, H., and Roelfsema, P.R. (2013). Distinct roles of the cortical layers of area V1 in figure-ground segregation. Curr. Biol. *23*, 2121–2129.
14. Fracasso, A., Petridou, N., and Dumoulin, S.O. (2016). Systematic variation of population receptive field properties across cortical depth in human visual cortex. Neuroimage *139*, 427–438.
15. Fracasso, A., Luijten, P.R., Dumoulin, S.O., and Petridou, N. (2018). Laminar imaging of positive and negative BOLD in human visual cortex at 7T. Neuroimage *164*, 100–111.
16. Muckli, L., De Martino, F., Vizioli, L., Petro, L.S., Smith, F.W., Ugurbil, K., Goebel, R., and Yacoub, E. (2015). Contextual feedback to superficial layers of V1. Curr. Biol. *25*, 2690–2695.
17. Koopmans, P.J., Barth, M., Orzada, S., and Norris, D.G. (2011). Multi-echo fMRI of the cortical laminae in humans at 7 T. Neuroimage *56*, 1276–1285.
18. Turner, R. (2002). How much cortex can a vein drain? Downstream dilution of activation-related cerebral blood oxygenation changes. Neuroimage *16*, 1062–1067.
19. Uludağ, K., and Blinder, P. (2018). Linking brain vascular physiology to hemodynamic response at ultra- high field MRI. Neuroimage *168*, 279–295.
20. Moerel, M., De Martino, F., Kemper, V.G., Schmitter, S., Vu, A.T., Uğurbil, K., Formisano, E., and Yacoub, E. (2018). Sensitivity and specificity considerations for fMRI encoding, decoding, and mapping of auditory cortex at ultra-high field. Neuroimage *164*, 18–31.
21. Serences, J.T., Ester, E.F., Vogel, E.K., and Awh, E. (2009). Stimulus-specific delay activity in human primary visual cortex. Psychol. Sci. *20*, 207–214.
22. Tong, F. (2013). Imagery and visual working memory: one and the same? Trends Cogn. Sci. *17*, 489–490.
23. Livingstone, M.S., and Hubel, D.H. (1984). Anatomy and physiology of a color system in the primate visual cortex. J. Neurosci. *4*, 309–356.
24. Self, M.W., van Kerkoerle, T., Goebel, R., and Roelfsema, P.R. (2017). Benchmarking laminar fMRI: Neuronal spiking and synaptic activity during top-down and bottom-up processing in the different layers of cortex. Neuroimage. Published online June 23, 2017. https://doi.org/10.1016/j.neuroimage.2017.06.045.
25. Nandy, A.S., Nassi, J.J., and Reynolds, J.H. (2017). Laminar organization of attentional modulation in macaque visual area V4. Neuron *93*, 235–246.
26. Ling, S., Pratte, M.S., and Tong, F. (2015). Attention alters orientation processing in the human lateral geniculate nucleus. Nat. Neurosci. *18*, 496–498.
27. Chen, R., Wang, F., Liang, H., and Li, W. (2017). Synergistic processing of visual contours across cortical layers in V1 and V2. Neuron *96*, 1388–1402.e4.
28. Hubel, D.H., and Wiesel, T.N. (1968). Receptive fields and functional architecture of monkey striate cortex. J. Physiol. *195*, 215–243.
29. Koyano, K.W., Takeda, M., Matsui, T., Hirabayashi, T., Ohashi, Y., and Miyashita, Y. (2016). Laminar module cascade from layer 5 to 6 implementing cue-to-target conversion for object memory retrieval in the primate temporal cortex. Neuron *92*, 518–529.
30. Tsao, D.Y., Freiwald, W.A., Knutsen, T.A., Mandeville, J.B., and Tootell, R.B.H. (2003). Faces and objects in macaque cerebral cortex. Nat. Neurosci. *6*, 989–995.
31. Kreiman, G., Hung, C.P., Kraskov, A., Quiroga, R.Q., Poggio, T., and DiCarlo, J.J. (2006). Object selectivity of local field potentials and spikes in the macaque inferior temporal cortex. Neuron *49*, 433–445.
32. Friston, K. (2005). A theory of cortical responses. Philos. Trans. R. Soc. Lond. B Biol. Sci. *360*, 815–836.

33. Rao, R.P.N., and Ballard, D.H. (1999). Predictive coding in the visual cortex: a functional interpretation of some extra-classical receptive-field effects. Nat. Neurosci. *2*, 79–87.
34. de Lange, F.P., Heilbron, M., and Kok, P. (2018). How Do Expectations Shape Perception? Trends Cogn. Sci. *22*, P764–P779.
35. Mumford, D. (1994). Neuronal architectures for pattern-theoretic problems. In Large-Scale Neuronal Theories of the Brain, C. Koch, and J.L. Davis, eds. (Cambridge, Massachusetts: MIT Press), pp. 125–152.
36. Bastos, A.M., Usrey, W.M., Adams, R.A., Mangun, G.R., Fries, P., and Friston, K.J. (2012). Canonical microcircuits for predictive coding. Neuron *76*, 695–711.
37. Huber, L., Handwerker, D.A., Jangraw, D.C., Chen, G., Hall, A., Stüber, C., Gonzalez-Castillo, J., Ivanov, D., Marrett, S., Guidi, M., et al. (2017). High-resolution CBV-fMRI allows mapping of laminar activity and connectivity of cortical input and output in human M1. Neuron *96*, 1253–1263.e7.
38. Brainard, D.H. (1997). The Psychophysics Toolbox. Spat. Vis. *10*, 433–436.
39. Engel, S.A., Rumelhart, D.E., Wandell, B.A., Lee, A.T., Glover, G.H., Chichilnisky, E.J., and Shadlen, M.N. (1994). fMRI of human visual cortex. Nature *369*, 525.
40. Sereno, M.I., Dale, A.M., Reppas, J.B., Kwong, K.K., Belliveau, J.W., Brady, T.J., Rosen, B.R., and Tootell, R.B. (1995). Borders of multiple visual areas in humans revealed by functional magnetic resonance imaging. Science *268*, 889–893.
41. Wandell, B.A., Dumoulin, S.O., and Brewer, A.A. (2007). Visual field maps in human cortex. Neuron *56*, 366–383.
42. Watson, A.B., and Pelli, D.G. (1983). QUEST: a Bayesian adaptive psychometric method. Percept. Psychophys. *33*, 113–120.
43. Poser, B.A., Koopmans, P.J., Witzel, T., Wald, L.L., and Barth, M. (2010). Three dimensional echo-planar imaging at 7 Tesla. Neuroimage *51*, 261–266.
44. Marques, J.P., Kober, T., Krueger, G., van der Zwaag, W., Van de Moortele, P.F., and Gruetter, R. (2010). MP2RAGE, a self bias-field corrected sequence for improved segmentation and T1-mapping at high field. Neuroimage *49*, 1271–1281.
45. Greve, D.N., and Fischl, B. (2009). Accurate and robust brain image alignment using boundary-based registration. Neuroimage *48*, 63–72.
46. van Mourik, T., Koopmans, P.J., and Norris, D.G. (2018). Improved cortical boundary registration for locally distorted fMRI scans. bioRxiv. https://doi.org/10.1101/248120.
47. Sethian, J.A. (1999). Level Set Methods and Fast Marching Methods: Evolving Interfaces in Computational Geometry, Fluid Mechanics, Computer Vision, and Materials Science (Cambridge University).
48. Waehnert, M.D., Dinse, J., Weiss, M., Streicher, M.N., Waehnert, P., Geyer, S., Turner, R., and Bazin, P.L. (2014). Anatomically motivated modeling of cortical laminae. Neuroimage *93*, 210–220.
49. Leprince, Y., Poupon, F., Delzescaux, T., Hasboun, D., Poupon, C., and Rivière, D. (2015). Combined Laplacian-equivolumic model for studying cortical lamination with ultra high field MRI (7 T). In 2015 IEEE 12th International Symposium on Biomedical Imaging (ISBI) (IEEE), pp. 580–583.
50. Meinshausen, N. (2008). Hierarchical testing of variable importance. Biometrika *95*, 265–278.

STAR★METHODS

KEY RESOURCES TABLE

REAGENT or RESOURCE	SOURCE	IDENTIFIER
Deposited Data		
Data and code	Donders Repository	http://hdl.handle.net/11633/di.dccn.DSC_3018028.02_957
Software and Algorithms		
MATLAB 2016a	MathWorks	https://www.mathworks.com; RRID: SCR_001622
FSL 5.0.9	FMRIB	https://fsl.fmrib.ox.ac.uk/fsl; RRID: SCR_002823
SPM 8	Wellcome Trust Centre for Neuroimaging	http://www.fil.ion.ucl.ac.uk/spm/; RRID: SCR_007037
FreeSurfer	FreeSurfer	https://surfer.nmr.mgh.harvard.edu/; RRID: SCR_001847
MrVista	Vista Lab	http://white.stanford.edu/software/
Laminar Analysis Toolbox	van Mourik et al., 2015, ISMRM, abstract	https://github.com/TimVanMourik/OpenFmriAnalysis
PsychToolBox	[38]	http://psychtoolbox.org/; RRID: SCR_002881

CONTACT FOR REAGENT AND RESOURCE SHARING

Further information and requests for resources should be directed to and will be fulfilled by the Lead Contact, Floris de Lange (floris.delange@donders.ru.nl).

EXPERIMENTAL MODEL AND SUBJECT DETAILS

Twenty-one healthy participants (one left-handed, eleven females, mean age 26.1, age range 19-46) with normal or corrected-to-normal vision completed the experiment. All gave written informed consent and the study was approved by the local ethics committees (CMO region Arnhem-Nijmegen, the Netherlands, and ethics committee of the University Duisburg-Essen, Germany). All participants (excluding one, who was an employed research assistant within the laboratory and volunteered to take part), were reimbursed for their time at the rate of €10 per hour. All participants completed a 1-hour retinotopic mapping session, a 1-hour psychophysics session, and a 1.5-hour working memory fMRI session.

METHOD DETAILS

Retinotopic Mapping

Retinotopic mapping data were acquired in a separate session using a Siemens 3T Trio MRI system (Siemens, Erlangen, Germany) using a 32-channel head coil and a T2*-weighted gradient-echo EPI sequence (TR 1500 ms, TE 40ms, 68 slices, 2 mm isotropic voxels, multi-band acceleration factor 4). One high resolution anatomical image was also acquired with a T1-weighted MP-RAGE sequence (TR 2300 ms, TE 3.03ms, 1 mm isotropic voxels, GRAPPA acceleration factor 2). Stimuli were programmed in MATLAB (MathWorks, Natick, MA) and presented using PsychToolbox [38] projected with a luminance-calibrated EIKI projector (resolution 1024 × 768, refresh rate 60 Hz) onto a rear-projection screen and viewed via a mirror (viewing distance ~90 cm). During the session subjects viewed high contrast, contrast-reversing (6 Hz) 90° rotating wedge and expanding ring stimuli that mapped responses to the central region of the visual field (radius 11 degrees of visual angle). Stimulus runs lasted 297 s (198 volumes), including eight full stimulus cycles and six starting dummy volumes that were discarded prior to analyses. Participants completed 3-5 runs of wedge stimuli and 1-2 runs of rings. During stimulus runs subjects were instructed to fixate on a small central fixation cross (10 pixels across) and press a button every time in changed color from red to green or green to red (30 switches per run). Anatomical data were automatically segmented into white matter, gray matter and CSF using FreeSurfer (http://surfer.nmr.mgh.harvard.edu/) and manually corrected. Functional data were analyzed using the phase encoded approach in MrVista (http://white.stanford.edu/software/). Polar angle and eccentricity data were visualized on an inflated cortical surface and the boundaries of V1, V2 and V3 were drawn manually using established criteria [39–41].

Psychophysical procedure

During the psychophysics session subjects completed the same visual working memory task (Figure 1) that was used in the working memory fMRI session. Sinusoidal grating stimuli were programmed in MATLAB (MathWorks, Natick, MA) and presented using

PsychToolbox [38] on a 24 inch BenQ XL2420T monitor (http://www.benq.eu/product/monitor/, resolution 1920 × 1080, refresh rate 120 Hz). Subjects viewed the stimuli from a chin rest mounted 60 cm from the display and were instructed to fixate on a central, black fixation dot (4 pixels across) at all times. Grating stimuli were presented centrally at 50% contrast on a mid-gray background behind an annulus mask (inner radius 1 degree, outer radius 8 degrees), and had a spatial frequency of 1 cycle/degree and random phase. Stimulus edges were softened with a linear ramp that started 0.5 degrees from the edge of the mask. On each trial, two sample gratings were presented with near-orthogonal orientations (45° ± 3° and 135° ± 3°), each presented for 0.2 s and separated by a 0.45 s interstimulus interval (ISI). Following another 0.45 s ISI, a cue (either a '1' or a '2') was presented centrally for 0.8 s to indicate which of the two sample orientations should be maintained in memory. An 11.5 s working memory interval followed, during which the subject had to maintain the cued orientation in memory. A probe was then presented for 0.5 s with an orientation that was slightly clockwise or counter-clockwise to the cued sample orientation. The relative orientation difference to the sample was controlled with a staircase function using QUEST [42] that targeted 75% correct performance. There was then a fixed-length 2 s response window for the subject to indicate whether the probe was clockwise or counter-clockwise to the cued sample with a button press. Feedback ('Correct' or 'Incorrect') was then presented centrally for 0.3 s. Missed responses were marked and reported as incorrect. The next trial then followed a 2 s intertrial interval. Subjects completed 120 trials, at which point the orientation discrimination threshold was recorded and used as a starting point for the staircase function in the fMRI task.

fMRI data acquisition

fMRI data for the working memory experiment were acquired using a Siemens Magnetom 7T MRI system (Siemens, Erlangen, Germany) using a commercial RF head coil (Nova Medical, Inc., Wilmington, MA, USA) with one transmit (TX) and 32 receive (RX) channels and a gradient coil (Type AS095, Siemens Healthcare, Erlangen, Germany) with 38 mT/m gradient strength and 200 mT/m/ms slew rate. Functional data were acquired with a T2*-weighted 3D gradient-echo EPI sequence [43] (TR 3408 ms, TE 28 ms, 0.8 mm isotropic voxels, 16° flip angle, 192 × 192 × 38.4 mm FOV, GRAPPA acceleration factor 4). Shimming was performed using the standard Siemens shimming procedure for 7T. Anatomical data were acquired with an MP2RAGE sequence [44] (TR 5000 ms, TE 2.04 ms, voxel size 0.8 mm isotropic, 240 × 240 mm FOV, GRAPPA acceleration factor 2) yielding two inversion contrasts (TI 900 ms, 4° flip angle and TI 3200 ms, 6° flip angle), which were combined to produce a T1-weighted image. We also acquired a T2-weighted HASTE scan that was used to identify the calcarine sulcus to aid functional slice positioning (TR 3230 ms, TE 67 ms, 7 coronal slices, 0.625 × 0.625 × 5.10 mm voxels). Stimuli were programmed and displayed using the same methods described for the psychophysics session onto a rear-projection screen using an EIKI (EIKI, Rancho Santa Margarita, CA) LC-X71 projector (1024 × 768 resolution, refresh rate 60 Hz), viewed via a mirror (view distance ~130 cm).

Each subject completed 3-4 runs of the working memory task. The task was identical to the psychophysics session, except the intertrial interval was extended to 10.8 s to allow time for the BOLD response to return to baseline between trials and align the beginning of the next trial with volume acquisition. Task difficulty was adjusted using a QUEST [38] staircase, which was given a starting estimate equal to the discrimination threshold measured from the subject's psychophysics session plus a 20% increment. 8 volumes were acquired per trial, with 20 trials in a single 555.5 s run. The first three volumes of each run were discarded to allow for signal stabilization.

After the working memory task, a high resolution anatomical image was acquired using the MP2RAGE sequence. Finally, subjects completed an orientation localizer scan that was used to measure voxel-wise orientation preference. Oriented gratings (same parameters as working memory stimuli, except the contrast was increased to 100%) were presented in an AoBo block design. Stimulus blocks were 13.6 s long (4 TR) and separated by rest blocks of the same length. During a stimulus block gratings were repeatedly presented with the same orientation at a rate of 2 Hz (250 ms on, 250 ms off). Phase was randomized for each stimulus presentation. Stimulus blocks alternated between blocks of clockwise gratings (45°) and blocks of counter-clockwise gratings (135°). A total of 30 stimulus blocks were presented in an 828.1 s run; the first 3 volumes were again discarded. During the scan subjects maintained fixation and pressed a button every time the fixation dot flashed white for 0.25 s (1 to 4 flashes per block).

Preprocessing of fMRI data

Functional volumes were cropped so that only the occipital lobe remained. This was to remove distortions in other brain areas further away from the shimming volume that was positioned in the occipital lobe, so that they could not affect coregistrations down the line. Cropped functional volumes were then spatially realigned within and then between runs using SPM8 (http://www.fil.ion.ucl.ac.uk/spm). Finally, data were highpass filtered using FEAT (fMRI Expert Analysis Tool) v6.00 (https://fsl.fmrib.ox.ac.uk/fsl) with a cut off of 28 s to remove low frequency scanner drift.

Coregistration of anatomical and functional data

7T anatomical data were segmented into white matter, gray matter and CSF using FreeSurfer's (http://surfer.nmr.mgh.harvard.edu/) automated procedure, the results of which were manually inspected and, if necessary, manually corrected. The white and gray matter surfaces were then aligned to the mean functional volume in two steps. First we computed a standard rigid body boundary based registration [45] between the cortical surface and the mean functional volume. Second, we fine-tuned the registration using a recursive registration algorithm that corrects for distortions in the phase encoding direction [46]. In brief, this algorithm applies a boundary based registration over multiple recursive iterations. With each iteration the mesh is split into two and each segment is registered to the functional volume independently. Each mesh segment is then split again and registered on the next iteration,

recursively fine-tuning the registration to correct for local distortions. In this case we used a total of 6 iterations for the recursive registration.

QUANTIFICATION AND STATISTICAL ANALYSIS

Definition of functional masks

We constrained our retinotopic regions of interest (ROIs), V1, V2 and V3, so that only the most selective voxels for our oriented grating stimuli were included in analyses. This comprised two steps. First, we constrained ROIs to only include voxels that responded to our visual stimuli. This was done by applying a temporal GLM to the preprocessed data from the orientation localizer scan using FEAT v6.00 (https://fsl.fmrib.ox.ac.uk/fsl). Blocks of clockwise and counter-clockwise stimuli were modeled separately as regressors of interest. Both stimulus regressors were contrasted against baseline to identify voxels that exhibited a significant response to our stimuli. Our retinotopic ROIs were then constrained to only include voxels that survived an uncorrected cluster correction ($z > 2.3$, $p < 0.05$).

The second step was to identify the orientation preference for each voxel within our constrained ROIs and generate separate masks for voxels that preferred clockwise and counter-clockwise orientations. The clockwise and counter-clockwise regressors were contrasted against each other to provide a t statistic for each voxel that described its orientation preference. From our constrained ROIs, we then took the 500 voxels with the most positive t values (prefer clockwise) and the 500 voxels with the most negative t values (prefer counter-clockwise) and used them to form separate masks. For each subject, therefore, we analyzed six functional masks, each containing 500 voxels, which included clockwise and counter-clockwise preference masks for V1, V2 and V3 (in a control analysis, we show that our results were not dependent on the number of voxels included in our masks; Figure S1). For one subject, there was an insufficient number of voxels in the constrained V2 and V3 ROIs for this process to be completed (i.e., < 1000 voxels), so we only analyzed V1 for this subject. As such, 20 of the 21 subjects contributed to analyses for V2 and V3.

Univariate approach to measuring working memory activity

Previous fMRI studies of visual working memory have used a multivariate approach that utilizes small but systematic biases in voxel orientation preference across visual cortex to decode the maintained orientation from brain activity during working memory [8]. Here, we used a univariate approach described by Albers et al. [10]. This approach monitors the response to the maintained and discarded items over time by measuring the response in voxels that prefer the maintained and discarded item separately. This results in a response difference between voxels populations during working memory, the size of which closely follows decoding accuracy over time [10]. An additional advantage of this univariate approach is that it was compatible with the spatial regression we used to estimate depth-specific responses (described in next section). This regression collapses across voxels within a region of interest, meaning in could only be followed by a univariate, but not a multivariate, analysis.

In order to make maximal use of the subtle voxel-wise orientation biases that support multivariate [8] and univariate [10] methods for assessing working memory fMRI activity, we designed a filter to weight functional data from each voxel by their orientation preference. This filter comprised a matrix of t values that described each voxel's orientation preference, derived from contrasting responses to clockwise and counter-clockwise gratings in the orientation localizer scan as described above. Data from voxels that preferred clockwise orientations were multiplied by their t values resulting from the clockwise > counter-clockwise contrast, while data from voxels that preferred counter-clockwise were multiplied by the t values from the counter-clockwise > clockwise contrast. This filter was applied to functional data from working memory scans by z scoring the data from each voxel and then multiplying the data with the matrix of stimulus selectivity t values. This filter maximized our sensitivity to small but reliable differences between voxels that preferred the maintained and discarded items during working memory [10] so that we might then examine how this difference is organized across cortical depths.

Estimation of laminar working memory activity

Depth-specific time courses were estimated for each functional mask using the spatial regression approach proposed by Van Mourik, Van Der Eerden and Norris (van Mourik et al., 2015, ISMRM, abstract) that has been described previously [9]. The segmented cortical mesh from FreeSurfer was divided into five depth bins: one white matter bin, three gray matter bins, and one CSF bin. Gray matter bins were computed using the level set method [47] and the procedures described by Waehnert et al. [48] to define three equivolume bins between the gray-white matter and gray matter-CSF boundaries. The gradient and curvature of the cortex were calculated using a Laplacian-equivolumic model [49] that accounts for the effect of local cortical curvatures on cortical depth bins. For each functional mask, we then calculated the proportion overlap of each voxel with the five bins we had defined. These depth weights were then used in a spatial GLM to estimate depth-specific BOLD responses.

Weighted functional data from each run of the working memory task were regressed against the depth weights for each voxel within the functional mask. This gave us the average time course across all voxels within the mask, separated into five depth bins (white matter, deep, middle and superficial gray matter, CSF), of which we further analyzed the three gray matter bins. For each functional mask we split the depth-specific time courses into separate segments comprising 8 volumes each, corresponding to a single trial. We then applied the following procedure to the data from each cortical depth bin to calculate depth-specific average 'preferred' and 'non-preferred' trial time courses. For a given trial, we used the average time course from the voxel population that preferred the cued orientation (i.e., prefer 45° voxels for a trial in which 45° was cued, prefer 135° voxels for a trial in which

135° was cued) as the preferred population time course. We then took the average time course for the same trial from the voxel population that preferred the other, non-cued orientation (i.e., prefer 135° voxels for a cue 45° trial, prefer 45° voxels for a cue 135° trial) as the non-preferred population time course. We completed this process for every trial, creating a preferred and non-preferred time course for every trial, and averaged across trials to calculate an average preferred trial time course and an average non-preferred trial time course. Average time courses collapsed across cortical depth are plotted in Figure 2A. We then examined the differential responses between preferred and non-preferred time courses specifically during the working memory delay period (highlighted in Figure 2A) and how it was organized across cortical depth (Figure 2B).

Finally, we conducted a control analysis to determine the laminar organization of a preferential response to visual presentation of a preferred orientation (i.e., externally generated signals) so that we could compare it to our working memory result. For this we turned to data from our orientation localizer, in which clockwise and counter-clockwise orientations were presented in a block design. Using the same methods just described, we computed average block time courses for blocks where the preferred orientation was presented, and blocks where the non-preferred orientation was presented (Figure 3A). Given that orientation preference weights were estimated using data from the orientation localizer scan, we did not contaminate this analysis by applying a weighted matrix derived from the same data. Instead, we chose to only examine how stimulus-selective bottom-up responses were organized across cortical depths, without applying the stimulus selectivity filter that was applied to working memory data.

Statistical testing

We quantified item-specific activity during visual working memory by examining the difference between preferred and non-preferred time courses during the working memory interval (6.8 and 10.2 s into the trial; see Figure 2A). We determined whether this effect was significant using a 2 × 2 repeated-measures ANOVA (factors: preferred/non-preferred and time point). We then examined how this difference was distributed across cortical depth (Figure 2B). We used a hierarchical statistical approach [50] to assess the laminar profile of working memory signals across ROIs. In this approach, a significant omnibus effect is required to assess difference between conditions. For example, a significant interaction between cortical depth and visual area would be required to justify examining how responses varied across depths within individual visual areas. Then, a significant main effect of cortical depth within an area would be required to justify examining differences between depths within that area. This approach controls the false alarm rate in hierarchical manner, by ensuring that one only examines comparisons that are statistically justifiable, rather than examining all possible comparisons.

We determined whether the laminar profile of working memory signals varied across visual areas using a 3 × 3 repeated-measures ANOVA (factors: visual area and depth). This revealed a significant interaction (see Results), so we further examined each visual area independently using one-way repeated-measures ANOVAs (factor: depth). In cases where there was a significant main effect of layer, we examined specific differences between layers using paired-samples t tests (this was the case only for V1). For all ANOVAs, if the assumption of sphericity was violated the degrees of freedom were adjusted using a Huynh-Feldt correction. To examine the laminar organization of bottom-up signals, we used the same statistical approach on time courses from the orientation localizer (Figure 3A). Again there was a significant interaction between cortical depth and visual area (see Results), so we interrogated each area independently with a one-way ANOVA. We then examined differences between cortical depths again only in visual areas where the was a significant main effect of depth; in this case only V3. Finally, we quantified whether the laminar organization of item-specific working memory activity (internally generated) was different from that of stimulus-selective activity during visual stimulation (externally generated) in V1. This was done by assessing the interaction in a 2 × 3 repeated-measures ANOVA (factors: working memory/visual stimulation and depth).

DATA AND SOFTWARE AVAILABILITY

The accession number for the data reported in this paper is Donders Research Data Repository: http://hdl.handle.net/11633/di.dccn.DSC_3018028.02_957